Through-dressing Wound Monitoring Based on The mmWave Sensor

Xiaoyu Zhang[1], Zhengxiong Li[2], Yanda Cheng[1], Chenhan Xu[3], Chuqin Huang[1], Emma Zhang[1], Ye Zhan[4], Wei Bo[1], Jun Xia[1], Wenyao Xu[1]
[1]University at Buffalo, [2]University of Colorado Denver, [3]North Carolina State University, [4]Linde Inc

ABSTRACT

Wound assessment is crucial for monitoring healing, but traditional methods require removing gauze, which can disrupt healing and increase infection risk. We introduce WavelyVision, an over-gauze wound assessment system based on the mmWave sensor. It detects skin moisture—a key wound condition indicator—by analyzing how mmWave signals change with moisture levels. To improve accuracy, WavelyVision uses a denoised imaging algorithm to reduce motion noise and separate skin signals from environmental interference. A physical model further enhances moisture estimation. Experiments show WavelyVision achieves high accuracy, with a moisture error of about 0.5% and an SSIM of about 0.9. These results demonstrate its potential for non-invasive wound monitoring.

ACM Reference Format:
Xiaoyu Zhang[1], Zhengxiong Li[2], Yanda Cheng[1], Chenhan Xu[3], Chuqin Huang[1], Emma Zhang[1], Ye Zhan[4], Wei Bo[1], Jun Xia[1], Wenyao Xu[1]. 2025. Through-dressing Wound Monitoring Based on The mmWave Sensor. In *The 3rd International Workshop on Human-Centered Sensing, Modeling, and Intelligent Systems (HumanSys '25), May 6–9, 2025, Irvine, CA, USA.* ACM, New York, NY, USA, 6 pages. https://doi.org/10.1145/3722570.3726884

1 INTRODUCTION

Millions of people are affected by wounds each year, with the United States reporting over 8 million cases annually, highlighting a substantial clinical and economic challenge [1]. The treatment of chronic wounds, like diabetic foot ulcers or those resulting from peripheral vascular disease, as well as acute wounds from injuries or surgical interventions, poses significant healthcare hurdles [2]. The cost associated with wound management in the U.S. exceeds $22 billion annually, emphasizing the critical need for efficient and innovative management strategies [3, 4].

Traditionally, wound evaluation methods in clinical settings involve ruler-based measurements and more invasive techniques such as injections of saline or gel [5, 6]. These approaches usually need close supervision by healthcare providers and are subject to errors lacking standardized, quantitative evaluations [7, 8]. Furthermore, the invasiveness of these techniques can lead to patient discomfort and elevate the risk of secondary complications [9]. The demand for a non-invasive, accurate, and objective method for wound assessment is therefore more pressing than ever.

Permission to make digital or hard copies of all or part of this work for personal or classroom use is granted without fee provided that copies are not made or distributed for profit or commercial advantage and that copies bear this notice and the full citation on the first page. Copyrights for components of this work owned by others than the author(s) must be honored. Abstracting with credit is permitted. To copy otherwise, or republish, to post on servers or to redistribute to lists, requires prior specific permission and/or a fee. Request permissions from permissions@acm.org.
HumanSys '25, May 6–9, 2025, Irvine, CA, USA
© 2025 Copyright held by the owner/author(s). Publication rights licensed to ACM.
ACM ISBN 979-8-4007-1609-9/2025/05.
https://doi.org/10.1145/3722570.3726884

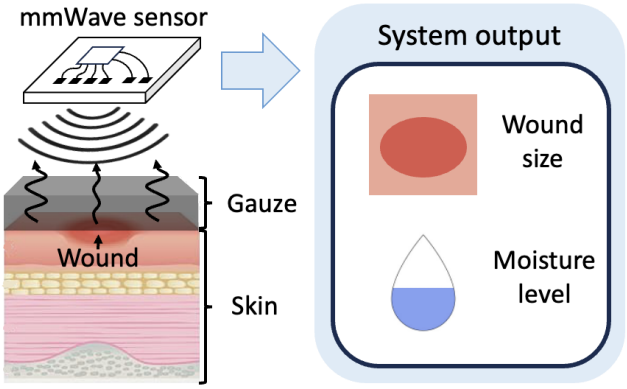


Figure 1: The WavelyVision system scans human wounds and provides a comprehensive assessment, including wound dimensions and moisture levels.

Initially, the approach to wound assessment employed non-invasive contact sensors that necessitated direct contact with the wound area. Ultrasound technology, for instance, has been used to probe wound conditions but requires physical contact that can introduce risks like secondary infections and increased discomfort for patients [10]. Subsequently, the development of non-contact methods, such as camera-based techniques, allowed for evaluating wounds without direct touch [11]. However, these methods cannot assess wounds covered by gauze, necessitating the exposure of wounds, which still poses an infection risk.

Advancing beyond these previous technologies, we present a novel technique: the mmWave-based WavelyVision method for assessing wounds through gauze. Illustrated in Figure 1, this method uses mmWave technology to detect changes in moisture content, a crucial biomarker in wound management [12]. The capability of mmWave signals to penetrate gauze allows for a non-intrusive assessment, maintaining the dressing intact and significantly lowering infection risks, thereby improving both patient safety and comfort.

2 HUMAN SKIN MODEL

Figure 2 offers a detailed depiction of the skin's layers, emphasizing components integral to the skin's hydration and moisture retention [13, 14]. The varying shades of blue in the illustration symbolize the water content within the skin layers. A deeper shade of blue typically represents a higher concentration of water. Human skin is composed of multiple layers, including the cuticle, epidermis, basement membrane, and dermis. Under normal conditions, the cuticle and basement membrane function as protective barriers, preventing internal water content from seeping to the surface. However, wounds compromise these protective layers, leading to water seepage and causing wounds to appear moist. The extent of

this moisture seepage depends on the severity of the wound. Light wounds typically damage only the upper layers of skin, resulting in minimal water loss. In contrast, severe wounds penetrate deeper into the dermis, where moisture levels are significantly higher. Consequently, severe wounds exhibit more pronounced moisture seepage, which is directly linked to higher external moisture levels. This variation in moisture serves as a vital biomarker for evaluating wound conditions and guiding treatment strategies.

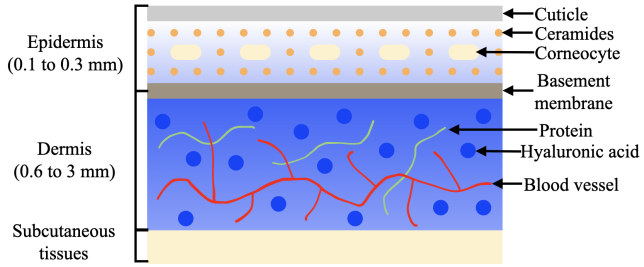


Figure 2: Human skin water distribution model.

3 WAVELYVISION SYSTEM DESIGN

The architecture of the WavelyVision system is depicted in Figure 3. Details of the steps will be discussed in the following sections.

3.1 mmWave Scanning

At the moment t, the mmWave signal can be represented by the function $f(t)$. To improve the spatial resolution captured by mmWave sensors, we employ the Synthetic Aperture Radar (SAR) technique. This method enables the sensor to simulate a much larger antenna aperture by moving across a two-dimensional (2D) plane, thereby enhancing image resolution. As depicted in Figure 4, the sensor moves over the 2D plane, collecting one chirp at each point in a uniform grid. The increments dx and dy represent the distances moved along the X and Y axes, respectively. At every point, the sensor gathers T data samples, allowing us to express the mmWave signal as $f(x, y, t)$, where x and y indicate the positions $x \cdot dx$ and $y \cdot dy$ on the X and Y axes, and t is the index for the T samples taken at each point. Here, x and y range from 1 to $\mathcal{X}$ and $\mathcal{Y}$ respectively, which represent the total number of sampling points along each axis.

3.2 Denoised mmWave Imaging

In this section, we introduce a method for mmWave imaging that aims to clarify and utilize the complex signal $f(x, y, t)$, which consists of reflections from various objects within the sensor's range. Our approach begins with applying a Fast Fourier Transform (FFT) to the time dimension of the signal. This conversion changes the original signal into a frequency spectrum or range bin profile $R(x, y, k)$, a technique known as Range-FFT. Here, the variable $k \in K$ serves as the range index within this profile. To focus effectively on the target, we select a specific range index k, determined by the distance d between the mmWave sensor and the target. This selection process is detailed in Equation (1), which strategically directs the sensor's focus to primarily gather data pertinent to the target. The focusing mechanism in the equation utilizes the *Slope*, which is the frequency shift rate over time, combined with the sampling rate F_s, the speed of light c, and the total number of collected samples T. This targeted approach helps in filtering out irrelevant data and enhancing the quality of information extracted from the target area.

$$k = \frac{Slope}{F_s} \times \frac{2d}{c} \times T. \tag{1}$$

The traditional mmWave imaging approach, as discussed in existing literature [15], presupposes that the distance between the mmWave sensor and the target remains constant across different scanning positions. This assumption is valid when the target is significantly distant from the sensor, making any positional shifts negligible in terms of changing distance. However, this is not the case in applications like human wound assessment, where the sensor operates at close proximity to the target. As illustrated in Figure 4, the sensor's distance to the target varies with its position; for instance, at (x_1, y_1) the sensor is closer to the target than at (x_2, y_2), resulting in $d_1 < d_2$. Such variation leads to different range indices ($k_1 \neq k_2$) when performing Range-FFT, which could potentially direct the sensor's focus towards environmental reflections rather than the actual target. To address these challenges, our denoised mmWave imaging algorithm modifies the target selection process by accounting for the actual distances measured from each scanning location. This ensures that the sensor consistently concentrates on the target across all positions. The output of this approach is a transformed mmWave signal, $R(x, y)|k = kxy$, where $x \in [1, \mathcal{X}]$ and $y \in [1, \mathcal{Y}]$, accurately representing information pertinent to the target.

Next, the transformed mmWave signal $R(x, y)|_{k=k_{xy}}$ is used to reconstruct the mmWave image $r(x, y)$ based on Equation (2) [16].

$$r(x, y) = |FT_{2D}^{-1}[FT_{2D}[R(x, y)|_{k=k_{xy}}]e^{-j\sqrt{4\omega^2-\omega_x^2-\omega_y^2}p_z}]|, \tag{2}$$

while FT_{2D} and FT_{2D}^{-1} are 2D Fourier Transform and Fourier Inverse Transform. p_z represents the distance from the target to the mmWave scanning plane, x and y are indexed in X and Y axes. $r(x, y), x \in [1, \mathcal{X}], y \in [1, \mathcal{Y}]$ is the mmWave channel gain of the target at the location of $(x \cdot dx, y \cdot dy, p_z)$, ω_x and ω_y are the space frequencies of the 2D plane.

3.3 Moisture Distribution Derivation

Using our denoised mmWave imaging algorithm, the 2D mmWave image is reconstructed to capture both the target and its surrounding environment. In the task of deriving moisture distribution from mmWave signal response images, we choose to use a Physics-Informed Neural Network (PINN) model primarily because it effectively addresses the challenge of data scarcity. The mapping between mmWave signal responses and skin moisture is governed by physical law, which is the interaction of electromagnetic waves with biological tissues. Obtaining a large amount of high-quality labeled data for training purely data-driven models is often impractical. PINNs overcome this limitation by embedding known physical constraints directly into the model, allowing it to learn accurate mappings even with limited labeled data. As illustrated in Figure 5, the PINN model is composed of segmentation and derivation parts, the details of the two parts are provided in the following sections.

3.3.1 mmWave Image Segmentation. To effectively differentiate the target from its surrounding environment in the denoised mmWave image, it is crucial to employ a segmentation model. We utilize

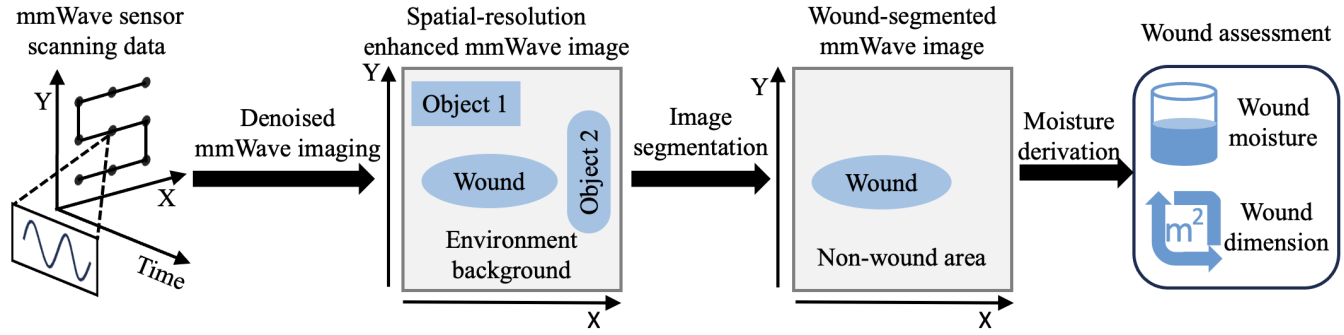


Figure 3: Framework of the WavelyVision system.

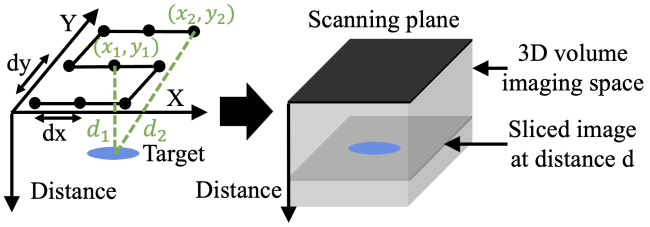


Figure 4: Diagram illustrating the use of a mmWave sensor to scan a human wound for assessment.

this model to discern the skin target by capitalizing on the distinct signal responses between the skin and other elements present in the environment, as detailed in [17]. In practice, this process involves inputting a 2D image $r(x, y)$ into the segmentation model. The output from this model is a masked image $m(x, y)$, where the dimensions match those of $r(x, y)$, and each pixel $m(x, y)$ assumes a binary value—either 0 or 1. Specifically, a pixel at (x, y) is assigned a value of $m(x, y) = 1$ if it is identified as part of the target area; otherwise, it is set to $m(x, y) = 0$. To enhance the accuracy and reliability of the segmentation process on mmWave images, we have incorporated a specialized loss function, $\mathcal{L}_S$, which is represented as follows:

$$\mathcal{L}_S = \frac{1}{\mathcal{X} \times \mathcal{Y}} \sum_{x,y} \mathcal{L}_{\text{pixel}}^{x,y}, \tag{3}$$

while $\mathcal{L}_{\text{pixel}}$ is a weighted combination of $\mathcal{L}_{\text{CE}}$ [18] and $\mathcal{L}_{\text{Dice}}$ [19] for each pixel:

$$\mathcal{L}_{\text{pixel}} = \delta_1 \mathcal{L}_{\text{CE}} + \delta_2 \mathcal{L}_{\text{Dice}}. \tag{4}$$

3.3.2 Physics-informed Moisture Derivation. In the context of human wound assessment based on the mmWave sensor, the channel gain r is a critical factor influenced predominantly by the reflection coefficient β and the transmission path loss α, as detailed in the study by Wu et al. [20]. During the operation of the sensor, mmWave signals are emitted towards the human skin and the reflected signals are captured. Since the transmission medium is air, which has a relatively minor effect on the path loss—owing to its low relative permittivity—the transmission path loss α is approximately 1, thus negligible in practical terms. The reflection coefficient β, on the other hand, quantifies the proportion of the mmWave signal that is reflected at the boundary between two different media. According to the Fresnel Equation, β is defined as $\beta = \frac{n_2 - n_1}{n_2 + n_1}$, where n_1 and n_2 are the refractive indices of the first and second media, respectively. In the specific application of wound assessment, the mmWave signal transitions from the air (first medium, with refractive index $n_1 \approx 1$) to human skin (second medium). The relationship between the mmWave signal channel gain r and the reflection coefficient β is described as follows:

$$r = c \cdot \alpha \cdot \beta = c \cdot \frac{n_{skin} - 1}{n_{skin} + 1}, \tag{5}$$

while c is a constant correlation coefficient and n_{skin} is the refractive index of the human skin. According to Equation (5), the mmWave signal channel gain r is only related to the refractive index of the human skin n_{skin}, which is the parameter that is the root of the relative dielectric constant ε [21], i.e., $n_{skin} = \sqrt{\varepsilon_{skin}}$.

In skin moisture sensing, we can regard the human skin as a mixture, which is composed of water and another component. Looyenga formula is a famous formula for the dielectric property of heterogeneous mixtures [22], it models the correlation between the moisture level V and the relative dielectric constant of the human epidermal ε, which is described in Equation (6) as follows:

$$V = \frac{(\varepsilon^{\frac{1}{3}} - \varepsilon_{other}^{\frac{1}{3}})}{(\varepsilon_{water}^{\frac{1}{3}} - \varepsilon_{other}^{\frac{1}{3}})}, \tag{6}$$

The moisture level V is defined as the mass ratio of water to the target. The relative dielectric constants of water (ε_{water}) and other components (ε_{other}) within the target are intrinsic properties of these materials and are thus constants. Consequently, the moisture level V is determined by the relative dielectric constant of the human skin (ε). According to Equations (2&5&6), there exists a correlation between the mmWave image values and the moisture level, establishing a direct link between these two important parameters.

$$V = \frac{\left(\left(\frac{2c}{c-r} - 1\right)^{\frac{2}{3}} - \varepsilon_{\text{other}}^{\frac{1}{3}}\right)}{\left(\varepsilon_{\text{water}}^{\frac{1}{3}} - \varepsilon_{\text{other}}^{\frac{1}{3}}\right)} = p\left(\frac{2c}{c-r} - 1\right)^{\frac{2}{3}} + q = pr' + q,$$

$$p = \frac{1}{\left(\varepsilon_{\text{water}}^{\frac{1}{3}} - \varepsilon_{\text{other}}^{\frac{1}{3}}\right)}, q = -\frac{\varepsilon_{\text{other}}^{\frac{1}{3}}}{\left(\varepsilon_{\text{water}}^{\frac{1}{3}} - \varepsilon_{\text{other}}^{\frac{1}{3}}\right)}, r' = \left(\frac{2c}{c-r} - 1\right)^{\frac{2}{3}}. \tag{7}$$

As shown in Figure 5, after obtaining the segmented mmWave image, a derivation module is employed to extract the p and q parameters, which are subsequently used to calculate the moisture

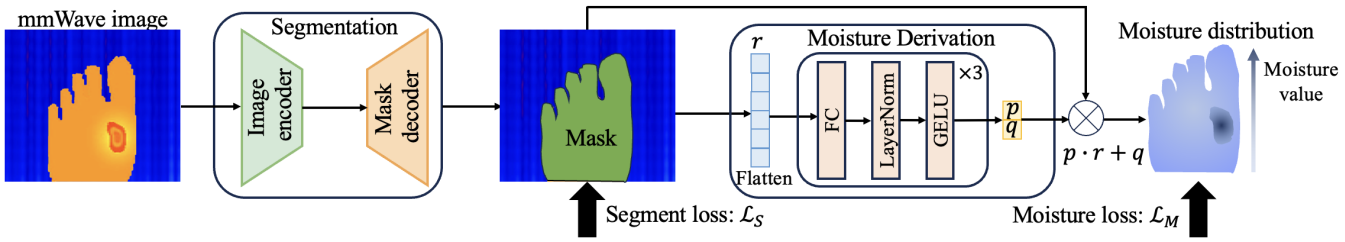


Figure 5: The framework of the Physics-Informed Neural Network (PINN) for evaluating moisture distribution.

distribution from the segmented mmWave image. Specifically, the loss function $\mathcal{L}_M$ is designed to guide the model in evaluating the moisture based on the physical relationship between the mmWave signal response and the moisture level:

$$\mathcal{L}_M = \frac{1}{\mathcal{X} \times \mathcal{Y}} \sum_{x,y} (V_G^{x,y} - p \times r'_{x,y} - q). \tag{8}$$

3.3.3 Total Loss Function of PINN model. The total loss function of our proposed PINN model is the combined loss function of the segmentation module and the derivation module, allowing the model to focus on the skin target area and accurately derive the moisture distribution. The combined loss function $\mathcal{L}$ is expressed as follows:

$$\mathcal{L} = \gamma_1 \mathcal{L}_S + \gamma_2 \mathcal{L}_M. \tag{9}$$

4 IMPLEMENTATION

4.1 System Integration

4.1.1 mmWave Scanning Kit. In the configuration depicted in Figure 6, the mmWave data acquisition is conducted using the TI AWR1642BOOST sensor. This sensor is mounted on a 2D motion platform comprised of two linear motion guides (THOMSON LINEAR MOTION SYSTEM) positioned at right angles to each other. The platform facilitates smooth, consistent movement of the sensor across a 2D plane at a predetermined velocity. As the sensor traverses this plane, it continually scans the target area, generating mmWave images. These images are produced using the specialized imaging algorithm described in Section 3.2. To synchronize the data collection accurately, an ELEGOO UNO R3 controller is employed. This controller emits stable square wave signals that serve dual functions: triggering the mmWave sensor to commence data sampling and commanding the 2D motion platform to initiate sensor movement. This dual-triggering mechanism ensures that each frame captured by the mmWave sensor is precisely aligned with its specific location on the 2D plane, based on the sensor's movement speed and the frame sampling rate.

4.1.2 System Parameter Setup. The 2D motion platform systematically transports the mmWave sensor across a grid at a constant rate of 50 mm/s on both the X and Y axes. This system utilizes a solitary transmitter (Tx) and receiver (Rx) configuration within the mmWave sensor for gathering data. The configuration is set to complete an FMCW frame in 0.025 seconds, which includes a single chirp. Given the chirp's duty cycle is approximately 0.3% of the total frame duration, this brief chirp length ensures the sensor effectively remains static during data capture at each scan point. The grid for 2D scanning comprises 51 discrete positions along both the X and Y dimensions, labeled as $\mathcal{X} = 51$ and $\mathcal{Y} = 51$. With a uniform stepping interval of 2 mm between each point, the entire scanning grid covers dimensions of $Dx = 100$ mm and $Dy = 100$ mm. Under these operational parameters, the full scanning process spans 102 seconds. The predefined distance between the sensor's scanning plane and the target is maintained at 30 mm. Throughout each chirp, the frequency of the mmWave sensor sweeps from 77 GHz to 81 GHz, thus utilizing a bandwidth of 4 GHz. The frequency slope, denoted as B, is established at 46.493 MHz/μs. Additionally, the sensor conducts uniform sampling 512 times during each chirp, capturing detailed frequency response data essential for high-resolution imaging.

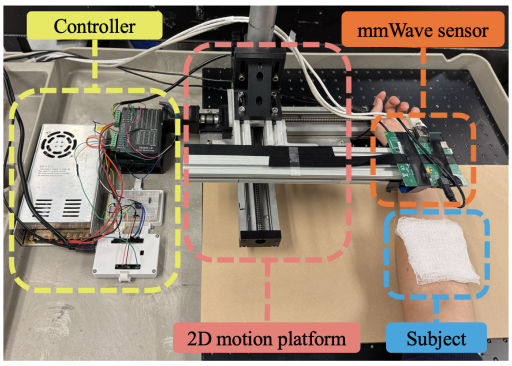


Figure 6: WavelyVision system prototype.

4.1.3 Training Parameter. The Physics-Informed Neural Network (PINN) model is implemented using PyTorch on an NVIDIA L40S GPU. The Adam optimizer is employed, with the learning rate set to 1e-3 and a multiplicative decay factor of 0.9 applied every 5 epochs. The loss function weights $\delta_1, \delta_2, \gamma_1, \gamma_2$ are set as 1, 1, 0.5, 1, respectively. The training process runs for 50 epochs with a batch size of 16.

4.2 Invivo Test Benchmark

Due to the limited access to real human wound samples, we simulate the abnormal moisture characteristics of wounds by applying ultrasound gel to the skin. This simulation approach builds upon established methodologies in wound research, where hydrogel-based materials have been widely adopted to mimic wound exudate properties [23, 24]. Compared to direct water application, the non-Newtonian fluid properties of ultrasound gel provide more stable hydration simulation with reduced evaporation effects, enabling reliable system evaluation during the scanning procedure. While acknowledging the inherent complexity of real wounds (e.g., healing stage variations, biochemical diversity), this standardized simulation protocol allows for controlled parametric studies of moisture detection sensitivity prior to clinical validation.

4.3 Groundtruth Moisture Distribution

To get the groundtruth of moisture distribution for the system training and testing, we harness the capabilities of Short-wave Infrared (SWIR) light. SWIR light, spanning the 0.9 - 1.7 μm wavelength range, has a limited penetration capacity but is notably absorbed by water molecules. Consequently, the wound with a higher moisture level will absorb more SWIR light, resulting in a decrease in reflected light intensity and, thus, a lower pixel value on the SWIR camera image. As shown in Figure 7, we establish a SWIR-based data collection platform and calibrate the SWIR camera to measure moisture distribution.

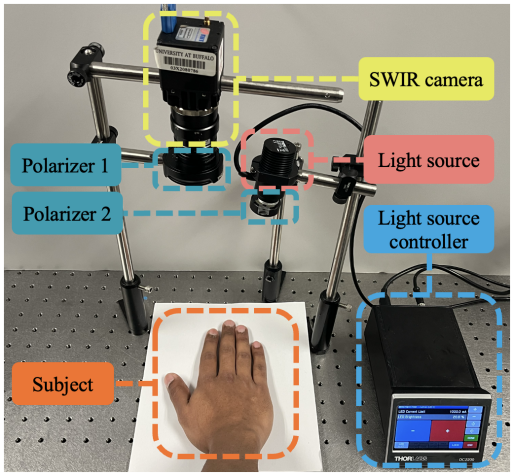


Figure 7: SWIR-based moisture distribution measurement platform.

4.4 Performance Metric

Mean moisture error (MME): The mean absolute error is used to quantify the moisture evaluation accuracy. For the output and groundtruth moisture distribution from the WavelyVision and SWIR systems, the predicted value v and groundtruth value $\hat{v}$ are obtained by calculating the mean value of the moisture distribution. As described in Equation (10), MME is computed by taking the absolute differences between the two values, summing all n absolute differences, and then dividing by the number of predictions made. MME is a non-negative value, which indicates the accuracy of our WavelyVision system in terms of moisture value estimation.

$$MAE = \frac{1}{n}\sum_{i=1}^{n}|v_i - \hat{v}_i|. \tag{10}$$

Structural Similarity Index (SSIM): The Structural Similarity Index is a metric used to assess the similarity between two images. The SSIM formula is typically expressed as:

$$SSIM(x,y) = \frac{(2\mu_x\mu_y + C_1)(2\sigma_{xy} + C_2)}{(\mu_x^2 + \mu_y^2 + C_1)(\sigma_x^2 + \sigma_y^2 + C_2)}, \tag{11}$$

where μ_x and μ_y are mean values of image x and image y, σ_x^2 and σ_y^2 are the variances, σ_{xy} is the Covariance between image x and image y, C_1 and C_2 are small constants to stabilize the division when denominators are close to zero, typically set as 6.5025 and 58.5225, respectively. SSIM values range from -1 to 1, where 1 indicates perfect similarity, 0 means no similarity, and negative values suggest inverse correlation.

5 EVALUATION

The wound condition is closely linked to the moisture level due to the water seepage effect. Therefore, wound assessment essentially involves evaluating the moisture distribution. In this section, we recruit 10 volunteers aged from 18 to 28, including 7 males and 3 females. Simulated wounds are created by applying ultrasound gel on various skin areas. For each participant, 50 data samples are collected. The training dataset is composed of data from 5 male and 2 female participants, while the remaining 2 male and 1 female participants are included in the testing dataset to evaluate the system's performance.

5.1 System Factor Analysis

As outlined in Section 3.2, the denoised mmWave imaging algorithm reduces motion noise during mmWave sensor scanning by synchronizing sensor-to-subject distance prior to imaging. To evaluate its effectiveness, the dataset is trained and tested on two system pipelines:

1). **Comparison system:** Conventional mmWave imaging algorithm [15] combined with a Physics-informed Neural Network (PINN) model.

2). **WavelyVision system (Ours):** Denoised mmWave imaging algorithm combined with the same PINN model.

System performance is assessed on the testing dataset using the SSIM metric described in Section 4.4. Specifically, we compare the similarity between the system's output moisture distribution and the groundtruth moisture distribution obtained from the SWIR camera. As shown in Table 1, our WavelyVision system, utilizing the denoised mmWave imaging algorithm, outperforms the comparison system in moisture distribution estimation. This improvement highlights the enhanced image quality provided by the denoised mmWave imaging algorithm.

Table 1: The mean structural similarity index measure (SSIM) results for moisture distribution estimation of different systems.

System Type	SSIM (Range from -1 to 1)
Comparison System	0.75
WavelyVision System	**0.88**

5.2 Over-gauze Wound Assessment

To examine the performance of the WavelyVision system in over-gauze wound assessment on real human skin, for the subjects in the testing dataset, we cover the simulated wounds with gauze of varying thicknesses, collect additional data, and evaluate the system's over-gauze performance. As shown in Table 2, the system's moisture distribution estimation remain largely unaffected by the presence of gauze, demonstrating the system's capability to perform reliable wound assessment under over-gauze conditions.

Table 2: The mean moisture error (MME) and mean structural similarity index measure (SSIM) results for moisture distribution estimation on real skin under different over-gauze conditions.

Gauze Thickness	MME	SSIM (Range from -1 to 1)
Without Gauze	0.54%	0.88
1-layer Gauze	0.5%	0.86
2-layer Gauze	0.57%	0.87

6 DISCUSSION

6.1 System Time Delay

The end-to-end latency of the WavelyVision system, which includes data collection, signal processing, and model prediction, currently reaches approximately 100 seconds per wound assessment. This duration is lengthy and underscores the need for time optimization to enhance the system's practicality. For example, during surgical wound monitoring, real-time feedback is crucial for guiding intraoperative adjustments. Similarly, in high-throughput wound care clinics, the system's efficiency has a direct impact on patient throughput and operational costs. Future improvements should concentrate on optimizing both the hardware (e.g., increased scanning speed) and software (e.g., more efficient neural networks), aiming to facilitate real-time wound assessment for these demanding contexts while preserving diagnostic accuracy.

6.2 Clinical Trial

The transition from controlled laboratory validation to clinical trials presents critical challenges for the WavelyVision system, particularly in addressing the inherent variability of real-world wound conditions—such as differences in tissue composition and healing stages—which may impact measurement consistency compared to idealized phantom models. To ensure clinical relevance, future trials must incorporate stratified patient cohorts (accounting for factors like skin pigmentation, wound age, and comorbidities) while maintaining standardized imaging protocols to isolate system performance from biological variability.

6.3 Portable Device Design

The breakthrough miniaturization of mmWave technology enables the development of WavelyVision as a potential portable wound monitoring device for home use. The small and light weight allow patients to conveniently perform daily wound assessments independently, without requiring professional assistance or complex setup procedures. However, to fully realize the potential of this portable solution for home healthcare applications, future development must focus on creating an advanced imaging algorithm capable of compensating for natural hand movements during operation. Such motion-robust algorithm would need to maintain diagnostic-quality scan accuracy despite the inevitable tremors and positional variations that occur during handheld use by non-professional users.

7 CONCLUSION

We introduce WavelyVision, a mmWave-based system for over-gauze wound assessment. It detects wound moisture using RF signals and reduces motion noise with a denoised imaging algorithm. A moisture model improves accuracy by linking mmWave signals to water content. Testing confirms its reliability, allowing wound checks without removing gauze, lowering infection risk. WavelyVision also shows potential for broader skin health monitoring.

REFERENCES

[1] Wound care. Available at: https://intermountainhealthcare.org/services/wound-care (accessed: 09.05.2024).

[2] Chronic wound affect. Available at: https://intermountainhealthcare.org/blogs/chronic-wounds-affect-65-million-in-us (accessed: 10.10.2024).

[3] Caroline E Fife and Marissa J Carter. Wound care outcomes and associated cost among patients treated in us outpatient wound centers: data from the us wound registry. *Wounds: a compendium of clinical research and practice*, 24(1):10–17, 2012.

[4] Koukab A Al-Gharibi, Sajana Sharstha, and Maria A Al-Faras. Cost-effectiveness of wound care: a concept analysis. *Sultan Qaboos University Medical Journal*, 18(4):e433, 2019.

[5] Sharon Baranoski and Elizabeth A Ayello. *Wound care essentials: Practice principles*. Lippincott Williams & Wilkins, 2008.

[6] II George Broughton, Jeffrey E Janis, and Christopher E Attinger. A brief history of wound care. *Plastic and reconstructive surgery*, 117(7S):6S–11S, 2006.

[7] Ruth Bryant and Denise Nix. *Acute and chronic wounds: current management concepts*. Elsevier Health Sciences, 2015.

[8] Health care. Available at: https://shcc.ufl.edu/services/primary-care/health-care-info-online/patient-education-wounds-caring-for/ (accessed: 05.12.2024).

[9] Cathy Thomas Hess. *Clinical guide to skin and wound care*. Lippincott Williams & Wilkins, 2012.

[10] Shuxin Li, Ali H Mohamedi, Jon Senkowsky, Ashwin Nair, and Liping Tang. Imaging in chronic wound diagnostics. *Advances in wound care*, 9(5):245–263, 2020.

[11] Lishuang Li, Yanan Sun, Honghui He, Gaiying He, Shuhua Ma, Weifeng Yang, and Yi Wang. Quantitative assessment of angiogenesis in skin wound healing by multi-optical imaging techniques. *Frontiers in Physics*, 10:894901, 2022.

[12] Zachary D Taylor, James Garritano, Shijun Sung, Neha Bajwa, David B Bennett, Bryan Nowroozi, Priyamvada Tewari, James W Sayre, Jean-Pierre Hubschman, Sophie X Deng, et al. Thz and mm-wave sensing of corneal tissue water content: in vivo sensing and imaging results. *IEEE transactions on terahertz science and technology*, 5(2):184–196, 2015.

[13] Rui Zhang, Qammer H Abbasi, and Akram Alomainy. Power distribution and performance analysis of terahertz communication in artificial skin. In *Proceedings of the Sixth Annual ACM International Conference on Nanoscale Computing and Communication*, pages 1–5, 2019.

[14] Rui Zhang, Ke Yang, Bin Yang, Najah Abed AbuAli, Mohammad Hayajneh, Mike Philpott, Qammer H Abbasi, and Akram Alomainy. Dielectric and double debye parameters of artificial normal skin and melanoma. *Journal of Infrared, Millimeter, and Terahertz Waves*, 40:657–672, 2019.

[15] Muhammet Emin Yanik and Murat Torlak. Millimeter-wave near-field imaging with two-dimensional sar data. *Proc. SRC Techcon*, (P093929), 2018.

[16] David M Sheen, Douglas L McMakin, and Thomas E Hall. Three-dimensional millimeter-wave imaging for concealed weapon detection. *IEEE Transactions on microwave theory and techniques*, 49(9):1581–1592, 2001.

[17] Alexander Kirillov, Eric Mintun, Nikhila Ravi, Hanzi Mao, Chloe Rolland, Laura Gustafson, Tete Xiao, Spencer Whitehead, Alexander C. Berg, Wan-Yen Lo, Piotr Dollár, and Ross Girshick. Segment anything. *arXiv:2304.02643*, 2023.

[18] T-YLPG Ross and GKHP Dollár. Focal loss for dense object detection. In *proceedings of the IEEE conference on computer vision and pattern recognition*, pages 2980–2988, 2017.

[19] Fausto Milletari, Nassir Navab, S Ahmadi Ahmadi, and V Net. Fully convolutional neural networks for volumetric medical image segmentation. In *Proceedings of the 2016 Fourth International Conference on 3D Vision (3DV)*, pages 565–571.

[20] Chenshu Wu, Feng Zhang, Beibei Wang, and KJ Ray Liu. msense: Towards mobile material sensing with a single millimeter-wave radio. *Proceedings of the ACM on Interactive, Mobile, Wearable and Ubiquitous Technologies*, 4(3):1–20, 2020.

[21] David L Andrews. *Photonics, Volume 2: Nanophotonic Structures and Materials*. John Wiley & Sons, 2015.

[22] H Looyenga. Dielectric constants of heterogeneous mixtures. *Physica*, 31(3):401–406, 1965.

[23] Shi Hua Tan, Dun An Cliff Chua, Je Re Jeremiah Tang, Carine Bonnard, David Leavesley, and Kun Liang. Design of hydrogel-based scaffolds for in vitro three-dimensional human skin model reconstruction. *Acta Biomaterialia*, 153:13–37, 2022.

[24] Alejandro Seijo-Rabina, Santiago Paramés-Estevez, Angel Concheiro, Alberto Pérez-Muñuzuri, and Carmen Alvarez-Lorenzo. Effect of wound dressing porosity and exudate viscosity on the exudate absorption: In vitro and in silico tests with 3d printed hydrogels. *International Journal of Pharmaceutics: X*, 8:100288, 2024.